PET/NIRF/MRI triple functional iron oxide nanoparticles

Jin Xie [a,c,1], Kai Chen [a,1], Jing Huang [a,b], Seulki Lee [a,c], Jinhua Wang [a], Jinhao Gao [a], Xingguo Li [b], Xiaoyuan Chen [a,c,*]

[a] *The Molecular Imaging Program at Stanford, Department of Radiology, Biophysics and Bio-X Program, Stanford University, Stanford, CA, USA*
[b] *Chemistry Department, Beijing University, Beijing, China*
[c] *Laboratory of Molecular Imaging and Nanomedicine (LOMIN), National Institute of Biomedical Imaging and Bioengineering (NIBIB), National Institutes of Health (NIH), Bethesda, MD 20892, USA*

ARTICLE INFO

ABSTRACT

Engineered nanoparticles with theranostic functions have attracted a lot of attention for their potential role in the dawning era of personalized medicine. Iron oxide nanoparticles (IONPs), with their advantages of being non-toxic, biodegradable and inexpensive, are candidate platforms for the buildup of theranostic nanostructures; however, progress in using them has been limited largely due to inefficient drug loading and delivery. In the current study, we utilized dopamine to modify the surface of IONPs, yielding nanoconjugates that can be easily encapsulated into human serum albumin (HSA) matrices (clinically utilized drug carriers). This nanosystem is well-suited for dual encapsulation of IONPs and drug molecules, because the encapsulation is achieved in a way that is similar to common drug loading. To assess the biophysical characteristics of this novel nanosystem, the HSA coated IONPs (HSA-IONPs) were dually labeled with ^{64}Cu-DOTA and Cy5.5, and tested in a subcutaneous U87MG xenograft mouse model. *In vivo* positron emission tomography (PET)/near-infrared fluorescence (NIRF)/magnetic resonance imaging (MRI) tri-modality imaging, and *ex vivo* analyses and histological examinations were carefully conducted to investigate the *in vivo* behavior of the nanostructures. With the compact HSA coating, the HSA-IONPs manifested a prolonged circulation half-life; more impressively, they showed massive accumulation in lesions, high extravasation rate, and low uptake of the particles by macrophages at the tumor area.

Published by Elsevier Ltd.

1. Introduction

Iron oxide nanoparticles (IONPs) are an important class of biomaterials with extensive usefulness in biomedicine, such as serving as contrast agents in magnetic resonance imaging (MRI) [1–4]. Recently, IONPs have been actively investigated as nanoplatforms on which to construct probes containing multiple imaging motifs [5–9], with several successful attempts already reported by us and other groups [10,11]. An even more ambitious goal is to load drugs into these nanosystems to achieve all-in-one theranostic agents that integrate manifold capabilities, including diagnostic imaging, drug delivery, and therapeutic monitoring. Theranostics offer great potential in the dawning era of personalized medicine

[12] by affording simultaneous therapy and monitoring. IONPs, with their advantages of non-toxicity, biodegradability and inexpensiveness, have been proposed as candidate materials for the buildup of theranostics, but progress has been limited. To work efficiently, the drug vehicles must have a reasonable circulation time, good lesion accumulation rate and high extravasation rate. However, conventional IONPs suffer from a relatively large size (hydrodynamic size >50 nm [13]) as well as mutual magnetic attraction, making them susceptible to acute hepatic accumulation and poor extravasation rates [13]. More critically, unlike other potential vehicles – such as carbon nanotubes [14], which afford unique molecule docking mechanisms – the IONP surface is unfavorable for drug loading. To date, most drug loading with IONPs has been achieved by covalent linking [13,15,16], which is inefficient and suboptimal for drug release.

One solution is to dope IONPs into molecular matrices with known drug loading capacity. Instead of serving as hosts, the IONPs are co-guests with drug molecules, and are both encapsulated. One such example was recently given by Yu et al. who utilized poly(TMSMA-r-PEGMA) to modify IONPs, and then loaded

---

* Corresponding author. Laboratory of Molecular Imaging and Nanomedicine (LOMIN), National Institute of Biomedical Imaging and Bioengineering (NIBIB), National Institutes of Health (NIH), Building 31, Room 1C22, Bethesda, MD 20892, USA. Tel.: +1 301 451 4246; fax: +1 301 480 1613.
   E-mail address: shawn.chen@nih.gov (X. Chen).
   [1] These authors contributed equally to this work.

them along with doxorubicin into the nanoconjugates, yielding agents with combined cancer imaging and therapy capacities [17]. However, the loading efficiency of such a system is not necessarily high, and its clinical translation prospective is unknown.

On the other hand, even though protein based vehicles, such as HSA, have long been utilized for drug delivery purposes [18], they have seldom been used to form theranositc agents with IONPs [11]. HSA has proven to be useful in extending the drug molecules' circulation half-lives and improving their tumor homing rate. Particularly, HSA-bound paclitaxel (Abraxane®) has demonstrated enhanced response rate and tumor regression compared with solvent based paclitaxel (PTX), and has been approved by FDA for chemotherapy. HSA drug loading is typically achieved by adding drugs in polar solvent into HSA aqueous solution [19]. This, however, is impractical with common IONPs, which are made by co-precipitation or pyrolysis, because they are either too hydrophilic or hydrophobic to form reliable complexes.

In the current study, we produced pyrolysis-derived IONPS with moderate polarity by modifying them with dopamine, and these were easily encapsulated into HSA matrices in a way similar to PTX loading. Such HSA-IONPs were labeled with Cy5.5 dye [20] and ^{64}Cu-DOTA chelates (Fig. 1), and injected into a subcutaneous U87MG xenograft mouse model. NIRF/PET/MRI imaging and histopathology were performed to understand the particles' pharmacokinetics and to evaluate their potential role as theranostic platforms.

2. Materials and methods

2.1. Nanoparticle preparation

Oleate coated IONPs with a diameter of 15 nm were obtained from Ocean NanoTech (Springdale, AR). For surface modification, about 5 mg of oleate coated nanoparticles was dispersed in 5 ml of chloroform, then 20 mg dopamine in 2 ml dimethyl sulfoxide (DMSO) was added into the solution, and the mixture was stirred to form a homogeneous solution. After heating at 70 °C for 1 h, the mixture was cooled down to room temperature, and the particles were collected via centrifugation at 15,000 g for 15 min. Subsequently, the particles were blown dry under nitrogen flow, and redispersed in DMSO with the aid of sonication. In parallel, 50 mg HSA was dissolved in 30 ml borate buffer (50 mM, pH 8.5) to make an HSA solution. With sonication, the nanoparticles in DMSO were added dropwise to the HSA solution. The solution was then centrifuged at 30,000 g for 20 min (3×) to remove the free HSA, and the collected particles were redispersed in phosphate buffered saline (PBS) and dialyzed against PBS (MWCO 10,000). A small portion of the aggregates was removed by passing the particles through a syringe filter (0.22 μm).

2.2. Labeling HSA-IONPs

The HSA-IONPs were buffer-changed with borate buffer (50 mM, pH 8.5) on a PD-10 column. For coupling, Cy5.5-NHS in DMSO was added into the particle solution at a 5:1 dye:HSA ratio, with the reaction carried out in darkness for 30 min. Subsequently, DOTA-NHS in DMSO was added, at a 5:1 DOTA:HSA ratio, and the reaction went on overnight in darkness. Details regarding the DOTA labeling have been reported elsewhere [21,22]. The solution was purified through a PD-10 column, and the solvent was exchanged to PBS buffer (pH 7.4).

2.3. Cell culture and animal model

A U87MG human glioblastoma cell line was purchased from the American Type Culture Collection (ATCC) and cultured with ATCC-formulated Eagle's Minimum Essential Medium (EMEM) in a cell culture incubator. Athymic nude mice were purchased from Harlan Laboratories. Approximately 5×10^6 U87MG cells were inoculated subcutaneously into the front flank of each mouse, and in vivo imaging was carried out 3 weeks after the inoculation (when the tumor size reached about 100 mm^3). All animal work was conducted following a protocol approved by the Stanford University Administrative Panel on Laboratory Animal Care (APLAC).

2.4. In vivo and ex vivo NIRF imaging

The mice were anesthetized with isoflurane (IsoFlo; Abbott Laboratories) and were i.v. injected with HSA-IONPs at a dose of 10 mg Fe/kg. The NIRF images were acquired on an IVIS 200 imaging system at 1 h, 4 h and 18 h post injection. At the end of the 18 h scan, the mice were sacrificed, and the tumors as well as the major organs were collected and subjected to ex vivo NIRF imaging with the IVIS 200 system.

2.5. Small-animal PET imaging

The details of small-animal PET imaging, and the region-of-interest (ROI) analysis have been reported previously [21,22]. The ^{64}Cu-labeled HSA-IONPs were purified with a PD-10 column and injected intravenously into the U87MG tumor-bearing mice at a dose of 10 mg Fe/kg. PET scans were performed with a microPET R4 rodent scanner (Siemens Medical Solutions) at 1 h, 4 h and 18 h post injection (p.i.) time points. For each scan, 3-dimensional ROIs were drawn over the tumor and organs on decay-corrected whole-body coronal images. The average radioactivity concentration was obtained from the mean pixel values within the ROI volume, and was converted to counts per milliliter per minute by using a predetermined conversion factor [21,23]. Given a tissue density of 1 g/mL, the counts per milliliter per minute were converted to counts per gram per minute, and the values were divided by the injected dose to obtain the imaging-ROI-derived percentage injected dose per gram (%ID/g). At the end of the 18 h scan, the mice were sacrificed, and the tumors as well as the major organs were collected and subjected to an ex vivo PET scan.

2.6. Small-animal MR imaging

HSA-IONPs were injected through the tail vein (10 mg Fe/kg) of the anesthetized mice. T2 weighted fast spin-echo images were acquired on a 7.0-T small-animal system (GE Healthcare), before and at 18 h after the particle injection, with the following parameters: TE 40 ms, TR 3000, thickness 1 mm, FOV 6 × 6, NEX 6.0, Echo 1/1. Signal intensities were measured in defined ROIs with Image J (National Institutes of Health).

2.7. Ex vivo fluorescence examination on the tumor sections

The U87MG tumor-bearing mice were injected with HSA-IONPs at a dose of 10 mg Fe/kg. At the 18 hp.i. time point, 200 μg fluorescein isothiocyanate (FITC)-labeled tomato lectin (Thermo Fisher Scientific, Rockford, IL) was injected, and the mice were sacrificed 10 min later. The tumors were harvested and put into optimal-cutting-temperature (o.c.t.) compound to prepare frozen tissue blocks. The tissue blocks were sectioned into 40 μm thick slices and stored in darkness until imaging. The fluorescence images were taken on an Axiovert 200M microscope (Carl Zeiss).

2.8. Prussian blue staining of tumor and major organ sections

Frozen organ blocks were sectioned into 10 μm slices. Before staining, the tissue slides were warmed up at room temperature for 20 min and fixed with ice-cold acetone for 5 min. Afterwards, they were dried and immersed in staining solution (a mixture of 20% hydrochloric acid and 10% potassium ferrocyanide solution in a 1:1 volume ratio) for 40 min. Next, the slides were washed gently with PBS and counterstained with eosin for 5 min. After that, they were dehydrated consecutively with 90%, 95% and 100% EtOH (3 min each), cleaned with xylene, and finally mounted with Permount medium.

2.9. Prussian blue/CD31 and Prussian blue/F4/80 double staining

Frozen U87MG tumor tissues were sectioned into 10 μm slices and stored at −80 °C. Before examination, the specimens were warmed up for 20 min at room temperature and fixed with ice-cold acetone for 5 min. After fixation, slides were incubated with 0.3% H_2O_2 solution in PBS for 10 min to block endogenous peroxidase activity, and were rinsed 3 times with PBS (2 min each). Primary rat anti-mouse CD31 antibody diluent (1:50) was subsequently applied to the tissue sections, and the incubation was carried on for 1 h in a humid chamber. After rinsing with PBS (3 × 2 min), a biotinylated anti-rat IgG secondary antibody solution (1:50) was applied, and the tissue was incubated for 30 min. The slides were rinsed again with PBS and were incubated with streptavidin-HRP solution for 30 min. After another washing cycle, the slides were developed with 3,3′-diaminobenzidine (DAB) substrate solution until the desired color intensity was reached. The resulting slides were subjected to Prussian blue staining with the procedure described above. Double staining of Prussian blue and F4/80 was conducted in a similar manner, except for changing the antibody to primary rat anti-mouse F4/80.

3. Results

3.1. Synthesis and characterization of HSA-IONPs

The IONPs were made from pyrolysis with a core diameter of 15 nm (Fig. 2a). The particles were coated with one layer of oleate and wouldn't disperse in water. To render them water-soluble, we conducted a two-step surface modification: in the first step, an excess amount of dopamine was utilized, which replaced the oleate coating by forming chelates with the surface Fe atoms [8,13,24];
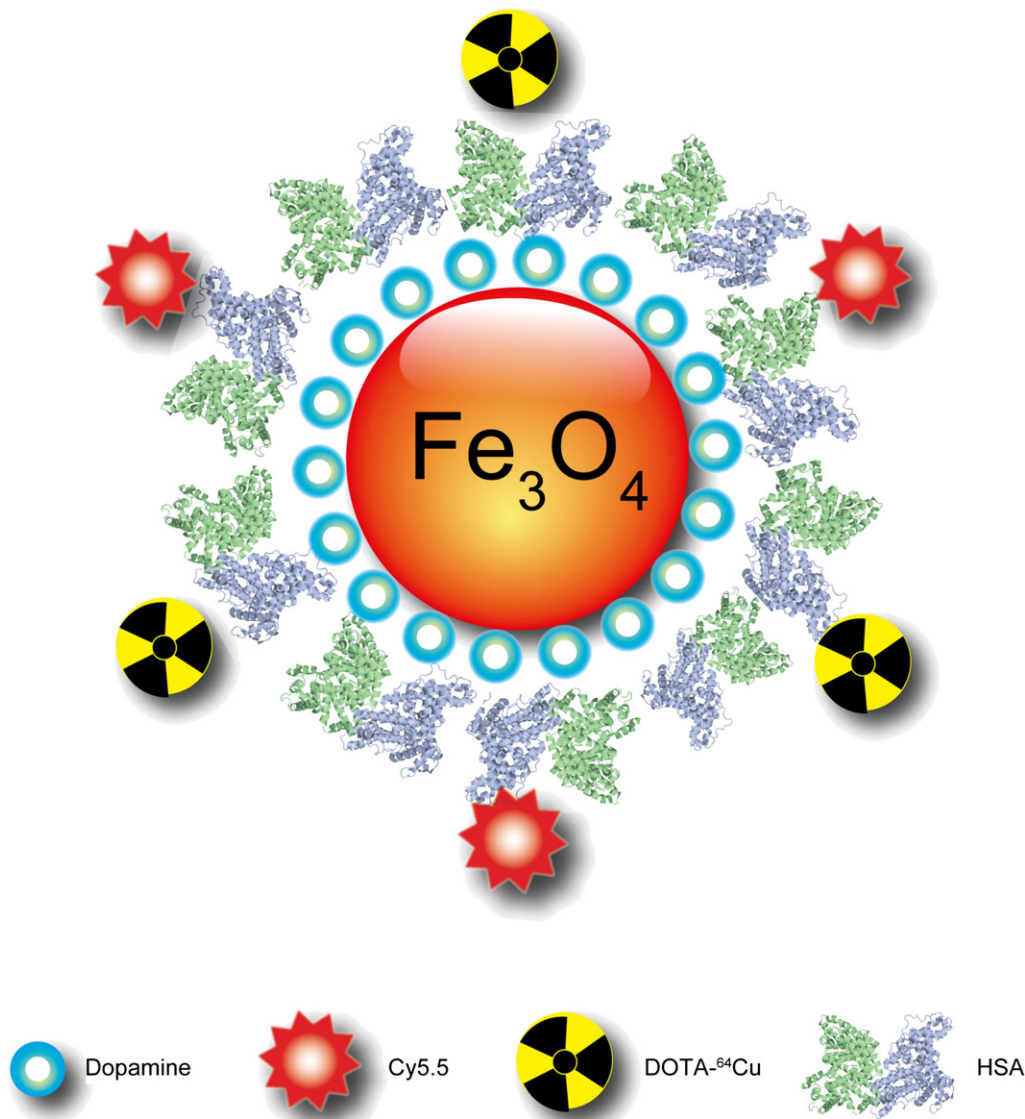
Fig. 1. Schematic illustration of the multi-funtional HSA-IONPs. The pyrolysis-derived IONPs were incubated with dopamine, after which the particles became moderately hydrophilic and could be doped into HSA matrices in a way similar to drug loading.

next, the dopamine modified particles in DMSO were added dropwise into HSA aqueous solution, where HSA was adsorbed onto the amine-rich particle surface (Fig. 1). The iron oxide cores remained almost intact throughout the modification, as little change in size or morphology was observed (Fig. 2b). The hydrodynamic size, on the other hand, increased from 19.0 ± 0.9 nm (hexane solution, ~ 2 nm oleate coating and 15 nm core) to 29.4 ± 1.2 nm (in PBS), which we attributed to the additional HSA coating (Fig. S1, Supporting Information). The HSA-IONPs are highly stable in aqueous environment, and showed little hydrodynamic size change when incubated in PBS buffer at 37 °C for 48 h (Fig. 2c). Although the details of the particle-HSA interaction are unknown at this stage, we postulate that the electrostatic forces between the albumin (pI 5.0) and the aminated particle surface play an important role. Compared with IONPs that are made from co-precipitation methods (such as Feridex), those made from pyrolysis are known to have better crystallinity, hence larger r_2 relaxivities [25]. To confirm this, we performed a phantom study and found that HSA-IONP has an r_2 of 313 mm^{-1} s^{-1}, much higher than that of Feridex (123 mm^{-1} s^{-1}) (Fig. 2d).

To assess the constitution of HSA-IONP particles, the protein and Fe concentrations were determined respectively by Bradford protein assay and inductively coupled plasma (ICP) spectrometry. The Fe concentration was further converted to particle concentration based on the assumption that each IONP was made of magnetite with a diameter of 15 nm and a density of 5.2 g/cm^3 [3]. The HSA/IONP mole ratio was determined to be about 10:1, i.e. on each IONP there are about ten HSA protein molecules (Fig. 1). Next, Cy5.5 and DOTA were coupled to the particle surface. In a previous study, we demonstrated that about 10 lysines from each HSA can be utilized for chemical coupling [20,26]. Herein, we mixed the nanoparticles with Cy5.5-NHS and DOTA-NHS at a 1:5:5 HSA:-Cy5.5:DOTA ratio to allow double labeling. According to the radio/fluorescent activities, it was estimated that there are about 20 Cy5.5/DOTA on each particle surface.

### 3.2. Small-animal NIRF/PET/MR triple imaging

The animal model was established by subcutaneously inoculating 5×10^6 U87MG cells into the front flank of each mouse, and
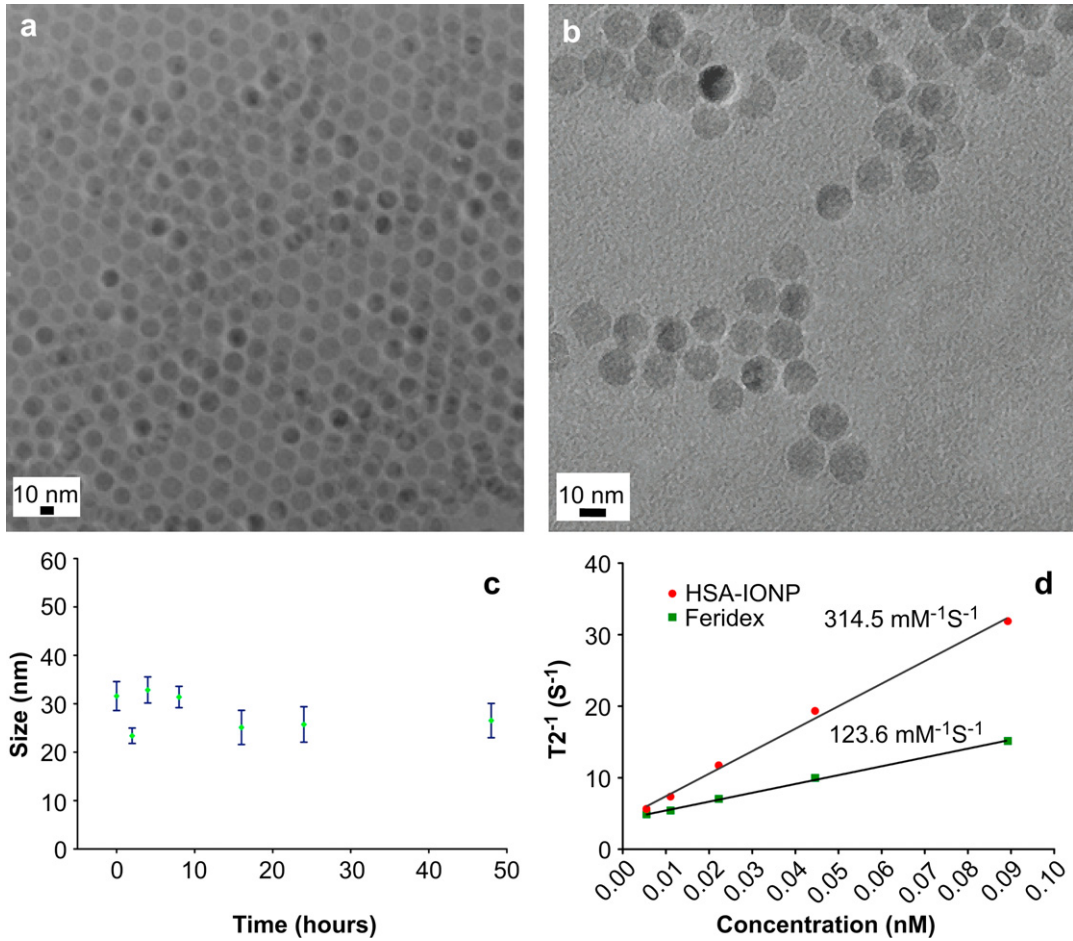
Fig. 2. (a) TEM of oleate coated IONPs in hexane. (b) TEM of the HSA-IONPs in water. (c) Hydrodynamic size change of the HSA-IONPs when incubating in PBS at 37 °C for 48 h, monitored by DLS. (d) r2 relaxivity evaluations with HSA-IONPs and Feridex.

by waiting until the tumor size reached 100 mm³. The HSA-IONPs were injected i.v. at a dosage of 10 mg Fe/kg, and PET/NIRF images were acquired 1 h, 4 h and 18 h post injection (Fig. 3). For NIRF results, a clear tumor delineation was observed at the 1 h time point, and the contrast improved over time, and the tumor/muscle ratio increased from 1.98 ± 0.20 at 1 h to 2.52 ± 0.27 at 4 h, and to 3.08 ± 0.28 at 18 h ($n = 3$/group) (Fig. 3a). A similar tumor homing

trend was observed in PET results, showing a gradually elevated tumor uptake of 5.46 ± 0.64, 6.11 ± 0.70 and $8.45 \pm 0.86\%$ ID/g at the 1, 4 and 18 h time points. Notably, compared with NIRF results, the PET imaging shows much higher tumor/muscle ratios of 4.55 ± 0.42, 5.36 ± 0.61 and 8.28 ± 0.90 at 1 h, 4 h and 18 h, respectively (Fig. 3b). Such improvement was mainly attributed to a cleaner background of PET [4]. In accord with these observations,
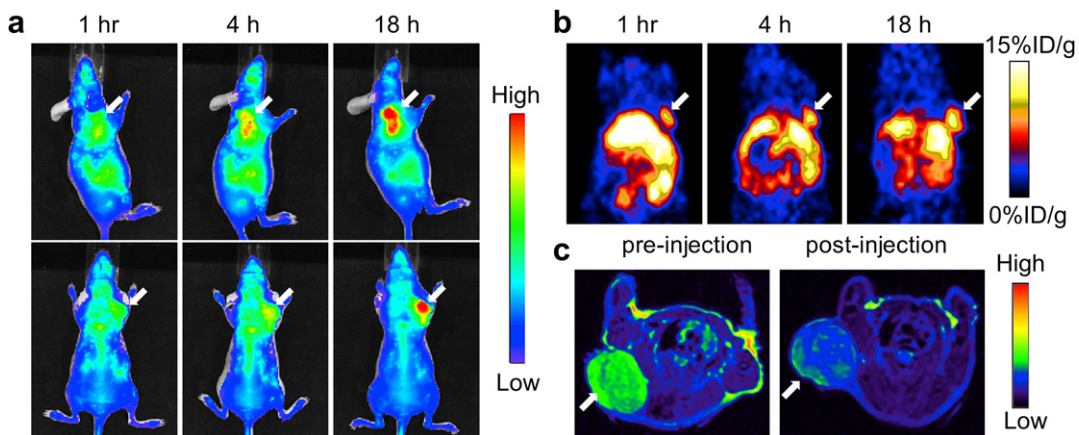
Fig. 3. (a) Representative *in vivo* NIRF images of mouse injected with HSA-IONPs. Images were acquired 1 h, 4 h and 18 h post injection. (b) *In vivo* PET imaging results of mouse injected with HSA-IONPs. Images were acquired 1 h, 4 h and 18 h post injection. (c) MRI images acquired before and 18 h post injection.
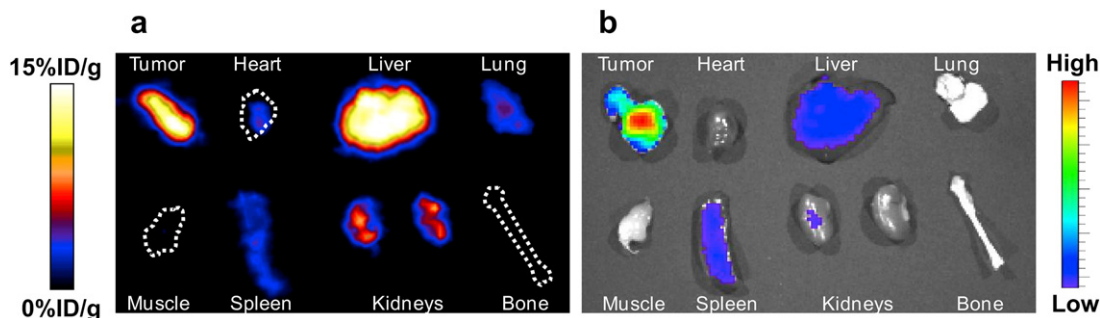
Fig. 4. (a) *Ex vivo* PET imaging on tumor and the major organs. (b) *Ex vivo* NIRF imaging on tumor and the major organs.

MRI scans performed pre- and 18 h post particle injection found a signal drop of $29.9 \pm 4.2\%$ at the tumor sites (Fig. 3c). A clear inhomogeneous particle distribution pattern was observed with MRI [27,28], but PET and NIRF results showed homogeneous intensities at the tumor area. Immediately after the 18 h scan, the mice were sacrificed and *ex vivo* PET and NIRF imaging were performed on the allograft tumors as well as on the major organs (Fig. 4). Besides substantial intensities from tumor, high tracer accumulation in the liver was also found by both imaging techniques, with liver/muscle ratios of 6.42 ± 0.78 and 28.2 ± 2.9 from NIRF and PET results, respectively. Again, such a discrepancy was mainly attributed to the relatively high background of NIRF imaging.

3.3. Histology studies

To improve our understanding of the particle distribution at the tissue and sub-tissue levels, we performed a series of immunostainings. An enrichment of the particles in tumor was found with Prussian blue staining, which correlated well with the *ex vivo* PET/NIRF results (Fig. 5a). Notably, the particles showed an inhomogeneous distribution pattern across the tumors, supporting the MRI observation. Next, using CD31 as a vasculature marker, Prussian blue and CD31 double staining were conducted on the tumor sections. As displayed in Fig. 6a, although some particles were found in the vascular lumen, most were found outside of the vessels, indicating a high extravasation rate. This observation was supported by a separate study, where Cy5.5 labeled HSA-IONPs were injected i.v. into U87MG bearing mice, followed by the administration of FITC-lectin, a blood vessel marker, at the 18 p.i.

time point. The *ex vivo* assessment of the tumor samples (Fig. 5b) found little correlation between the particles (red) and the vasculature (green); rather, most of the particles stayed outside of vasculature. It is worth noting that, due to limited resolution, only the spots with particle aggregates can be seen by fluorescence microscopy. Taking that into account, the *ex vivo* fluorescence examination demonstrated a particle distribution pattern similar to that of the Prussian blue staining results. To further evaluate whether the trapping of particles at the tumor site was caused by macrophage uptake, Prussian blue and F4/80 double staining were performed on the tumor sections (Fig. 6b). Although some co-localization between the two staining results was found, the retention of most of the particles was found to be non-related to macrophage uptake.

4. Discussion

IONPs must have moderate hydrophobicity in order to be doped into HSA matrices. Unfortunately, traditional IONPs made from either co-precipitation methods or pyrolysis methods do not have this property. In this study, by simply incubating with dopamine, we obtained an IONP formula that can be dispersed in polar solvents, such as DMSO, but is not strongly water-soluble. In a way that resembles a drug loading process, these particles were added into HSA solution, where they adsorb one layer of HSA, yielding complexes that are stable under physiological conditions. Even just from the particle preparation perspective, this method is meaningful, affording an easy, reliable and high-throughput way to make highly stable IO nanoconjugates. More importantly, by sharing
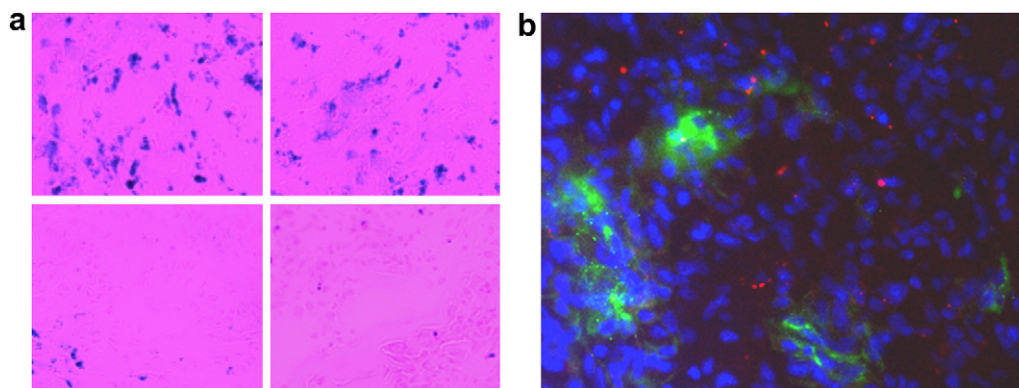

Fig. 5. (a) Prussian blue staining on tumor sections. Blue spots, representing the Fe contents, were found across the tumor and the distribution was found in an inhomogeneous pattern. (b) *Ex vivo* examination of tumor sections by fluorescence microscope. Cy5.5 labeled HSA-IONPs were i.v. injected into mice. Then at the 18 h time point, FITC labeled tomato lectin was injected, and the mice were sacrificed 10 min later. The overlaid image was constructed by MataMorph Imaging Processing software. The red, green and blue colors represent Cy5.5-HSA-IONPs, FITC-lectin and DAPI, respectively.
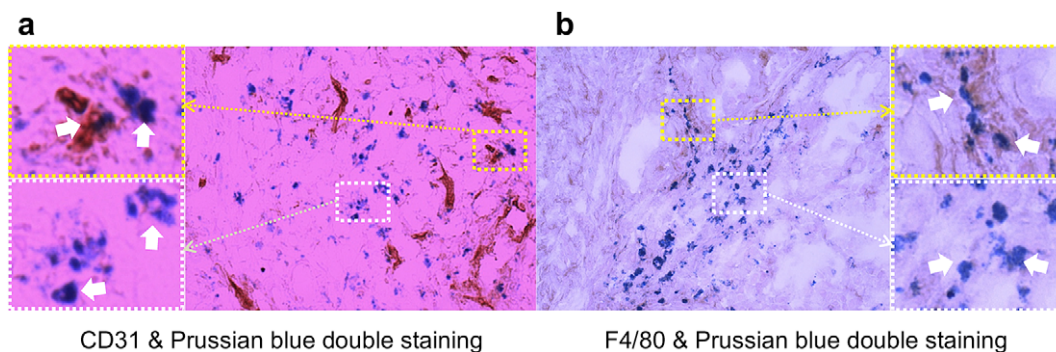
Fig. 6. (a) CD31 and Prussian blue double staining of the tumor samples. Some particles were found within the vessels (upper left), while many others managed to extravasate (lower left). (b) F4/80 and Prussian blue double staining of the tumor samples. Although some particles were found within macrophages (upper right), most of them were found independent of macrophages (lower right).

a similar doping process, these IONPs have the potential to be co-loaded with drug molecules to yield theranostic agents.

To evaluate the pharmacokinetics, the HSA-IONPs were dually labeled with both ^{64}Cu-DOTA chelator and Cy5.5 to make them MRI/PET/NIRF triple active. This approach was based on the consideration that each of these three modalities has advantages, and an integrated approach may lead to synergistic benefits [29]. For instance, MRI offers a high spatial resolution and, as proven in this study, and can provide a better description of the particle distribution pattern than either PET or NIRF. However, MRI has the issue of limited sensitivity. To compensate for this drawback, PET and NIRF reporters were added. Between these two, PET provides a better signal-to-noise ratio. NIRF, on the other hand, can be visualized both *in vivo* by an IVIS system and *ex vivo* by fluorescence microscopy, playing a unique role of bridging the *in vivo* and histological observations. By combining the information gathered from all the aspects, we confirmed that the HSA-IONPs have not only a high retention rate, but also a good extravasation rate and a low macrophage uptake rate at the tumor area. All of these observations are encouraging, considering the ultimate goal of using these particles as theranositc nanoplatforms.

We attributed the profound tumor retention of the particles mainly to the more permeable vasculature environment at the tumor site, i.e. the EPR effect (enhanced permeability and retention effect) [20]. Also, the interaction of the HSA sheath with cell surface glycoprotein (gp60) receptor (albondin) and/or SPARC (secreted protein acid and rich in cysteine) should have played a role, which facilitated the transportation of the particles [20,30–32]. But neither of the mechanisms would have worked without a reason-able circulation half-life of the particles. Compared with traditional formulas, the HSA-IONPs appear to be less provocative to the immune secretion and possess prolonged circulation half-life, probably due to their HSA protection. In one analysis, HSA-IONPs and Feridex at the same dosage (10 mg Fe/kg) were injected i.v. into mice, and MRI was used to monitor the signal changes in liver. For Feridex, the signal drop in liver maximized at 1 h and started regaining at the 2 h time point. On the contrary, in the HSA-IONP group, the contrast enhanced gradually and the effect lasted for more than 24 h, indicating a much improved circulation half-life (Fig. S2, Supporting Information). It is worth noting that ICP emission spectrometry, a potent means frequently used to evaluate inorganic nanoparticle biodistribution [33,34], is not applicable in this study, due to the high contribution of endogenous Fe. Also, although researchers have utilized Fe isotope as precursors in making IONPs [35], these efforts were limited to particles made from co-precipitation and are technically challenging for applica-tion to pyrolysis-based IONP preparation and analysis.

One major concern of this study is the possibility that the HSA sheath, although seemingly stable in the *in vitro* analysis, may detach from the particle surface in the complex *in vivo* environment and lead to false-positive observations. However, the *ex vivo* fluo-rescence examination (Fig. 5b) showed a particle distribution pattern that was very similar to the Prussian blue staining results, suggesting that coating detachment was not severe, if it occurred.

The results of this study show the potential benefits of this system in a theranostic context. The preliminary tests have confirmed that drug molecules, such as PTX, can be co-loaded into such nanosystems without significantly changing the particles' physical properties (Fig. S1, Supporting Information). Due to the large number of variables, such as original particle size, particle to drug ratio, loading buffer pH, etc., it will be non-trivial to optimize formulas (e.g., optimal drug loading rate and stability) with even one particular drug molecule. It was worth pointing out that, although IONPs may occupy certain binding sites of HSA, they may not necessarily compromise the loading efficacy of the drug molecules. An amine-rich coating layer could even enhance the particles' ability to interact electrostatically with drug molecules. Furthermore, it may be possible to incorporate some molecules for which HSA is not a favorable excipient, such as siRNA, into such nanosystem.

5. Conclusions

In the current work, we introduced a two-step, dopamine-plus-HSA strategy to yield stable nanoconjugates. Unlike the traditional IONP surface modification method, this approach allows the particles to be loaded into HSA matrices in a way that resembles Abraxane preparation. Imaging and histological examinations found that the particles have a good retention rate and a high extravasation rate at the tumor sites, due it is believed to the compact HSA coating. In addition, it was confirmed that particle accumulation at the tumor sties is not caused by macrophage uptake.

Appendix. Supplementary data

Supplementary data associated with this article can be found in the online version, at doi:10.1016/j.biomaterials.2010.01.010.

Appendix

Figures with essential colour discrimination. Most of the figures in this article may be difficult to interpret in black and white. The full colour images can be found in the on-line version, at doi:10.1016/j.biomaterials.2010.01.010.

References

[1] Jun YW, Huh YM, Choi JS, Lee JH, Song HT, Kim S, et al. Nanoscale size effect of magnetic nanocrystals and their utilization for cancer diagnosis via magnetic resonance imaging. J Am Chem Soc 2005;127:5732–3.

[2] Lee HY, Lee SH, Xu CJ, Xie J, Lee JH, Wu B, et al. Synthesis and characterization of PVP-coated large core iron oxide nanoparticles as an MRI contrast agent. Nanotechnology 2008;19:165101 (6pp).

[3] Xie J, Chen K, Lee HY, Xu C, Hsu AR, Peng S, et al. Ultrasmall c(RGDyK)-coated Fe_3O_4 nanoparticles and their specific targeting to integrin alpha(v)beta3-rich tumor cells. J Am Chem Soc 2008;130:7542–3.

[4] Cai W, Chen X. Nanoplatforms for targeted molecular imaging in living subjects. Small 2007;3:1840–54.

[5] Montet X, Montet-Abou K, Reynolds F, Weissleder R, Josephson L. Nanoparticle imaging of integrins on tumor cells. Neoplasia 2006;8:214–22.

[6] Nahrendorf M, Zhang H, Hembrador S, Panizzi P, Sosnovik DE, Aikawa E, et al. Nanoparticle PET-CT imaging of macrophages in inflammatory atherosclerosis. Circulation 2008;117:379–87.

[7] Choi JS, Park JC, Nah H, Woo S, Oh J, Kim KM, et al. A hybrid nanoparticle probe for dual-modality positron emission tomography and magnetic resonance imaging. Angew Chem Int Ed Engl 2008;47:6259–62.

[8] Xu C, Xie J, Ho D, Wang C, Kohler N, Walsh EG, et al. Au-Fe3O4 dumbbell nanoparticles as dual-functional probes. Angew Chem Int Ed Engl 2008;47:173–6.

[9] Lee S, Chen X. Dual-modality probes for in vivo molecular imaging. Mol Imaging 2009;8:87–100.

[10] Lee HY, Li Z, Chen K, Hsu AR, Xu C, Xie J, et al. PET/MRI dual-modality tumor imaging using arginine-glycine-aspartic (RGD)-conjugated radiolabeled iron oxide nanoparticles. J Nucl Med 2008;49:1371–9.

[11] Lee JH, Lee K, Moon SH, Lee Y, Park TG, Cheon J. All-in-one target-cell-specific magnetic nanoparticles for simultaneous molecular imaging and siRNA delivery. Angew Chem Int Ed Engl 2009;48:4174–9.

[12] Park K, Lee S, Kang E, Kim K, Choi K, Kwon IC. New generation of multifunctional nanoparticles for cancer imaging and therapy. Adv Funct Mater 2009;19:1553–66.

[13] Xie J, Huang J, Li X, Sun S, Chen X. Iron oxide nanoparticle platform for biomedical applications. Curr Med Chem 2009;16:1278–94.

[14] Liu Z, Chen K, Davis C, Sherlock S, Cao Q, Chen X, et al. Drug delivery with carbon nanotubes for in vivo cancer treatment. Cancer Res 2008;68:6652–60.

[15] Kohler N, Fryxell GE, Zhang MQ. A bifunctional poly(ethylene glycol) silane immobilized on metallic oxide-based nanoparticles for conjugation with cell targeting agents. J Am Chem Soc 2004;126:7206–11.

[16] Kohler N, Sun C, Fichtenholtz A, Gunn J, Fang C, Zhang MQ. Methotrexate-immobilized poly(ethylene glycol) magnetic nanoparticles for MR imaging and drug delivery. Small 2006;2:785–92.

[17] Yu MK, Jeong YY, Park J, Park S, Kim JW, Min JJ, et al. Drug-loaded superparamagnetic iron oxide nanoparticles for combined cancer imaging and therapy in vivo. Angew Chem Int Ed Engl 2008;47:5362–5.

[18] Gradishar WJ, Tjulandin S, Davidson N, Shaw H, Desai N, Bhar P, et al. Phase III trial of nanoparticle albumin-bound paclitaxel compared with polyethylated castor oil-based paclitaxel in women with breast cancer. J Clin Oncol 2005;23:7794–803.

[19] Gradishar WJ. Albumin-bound paclitaxel: a next-generation taxane. Expert Opin Pharmacother 2006;7:1041–53.

[20] Chen K, Xie J, Chen X. RGD-human serum albumin conjugates as efficient tumor targeting probes. Mol Imaging 2009;8:65–73.

[21] Cai W, Wu Y, Chen K, Cao Q, Tice DA, Chen X. In vitro and in vivo characterization of ^{64}Cu-labeled Abegrin, a humanized monoclonal antibody against integrin alpha v beta 3. Cancer Res 2006;66:9673–81.

[22] Cai W, Olafsen T, Zhang X, Cao Q, Gambhir SS, Williams LE, et al. PET imaging of colorectal cancer in xenograft-bearing mice by use of an 18F-labeled T84.66 anti-carcinoembryonic antigen diabody. J Nucl Med 2007;48:304–10.

[23] Cai W, Chen K, He L, Cao Q, Koong A, Chen X. Quantitative PET of EGFR expression in xenograft-bearing mice using 64Cu-labeled cetuximab, a chimeric anti-EGFR monoclonal antibody. Eur J Nucl Med Mol Imaging 2007;34:850–8.

[24] Xie J, Xu C, Kohler N, Hou Y, Sun S. Controlled PEGylation of monodisperse Fe_3O_4 nanoparticles for reduced non-specific uptake by macrophage cells. Adv Mater 2007;19:3648–52.

[25] Lee JH, Huh YM, Jun Y, Seo J, Jang J, Song HT, et al. Artificially engineered magnetic nanoparticles for ultra-sensitive molecular imaging. Nat Med 2007;13:95–9.

[26] Temming K, Meyer DL, Zabinski R, Dijkers EC, Poelstra K, Molema G, et al. Evaluation of RGD-targeted albumin carriers for specific delivery of auristatin E to tumor blood vessels. Bioconjug Chem 2006;17:1385–94.

[27] Ferrero E, Zocchi MR, Magni E, Panzeri MC, Curnis F, Rugarli C, et al. Roles of tumor necrosis factor p55 and p75 receptors in TNF-alpha-induced vascular permeability. Am J Physiol Cell Physiol 2001;281:C1173–9.

[28] Brett J, Gerlach H, Nawroth P, Steinberg S, Godman G, Stern D. Tumor necrosis factor/cachectin increases permeability of endothelial cell monolayers by a mechanism involving regulatory G proteins. J Exp Med 1989;169:1977–91.

[29] Cherry SR. Multimodality in vivo imaging systems: twice the power or double the trouble? Annu Rev Biomed Eng 2006;8:35–62.

[30] Desai N, Trieu V, Yao Z, Louie L, Ci S, Yang A, et al. Increased antitumor activity, intratumor paclitaxel concentrations, and endothelial cell transport of cremophor-free, albumin-bound paclitaxel, ABI-007, compared with cremophor-based paclitaxel. Clin Cancer Res 2006;12:1317–24.

[31] John TA, Vogel SM, Tiruppathi C, Malik AB, Minshall RD. Quantitative analysis of albumin uptake and transport in the rat microvessel endothelial monolayer. Am J Physiol Lung Cell Mol Physiol 2003;284:L187–96.

[32] Porter PL, Sage EH, Lane TF, Funk SE, Gown AM. Distribution of SPARC in normal and neoplastic human tissue. J Histochem Cytochem 1995;43:791–800.

[33] Qian X, Peng XH, Ansari DO, Yin-Goen Q, Chen GZ, Shin DM, et al. In vivo tumor targeting and spectroscopic detection with surface-enhanced Raman nanoparticle tags. Nat Biotechnol 2008;26:83–90.

[34] Lee HA, Imran M, Monteiro-Riviere NA, Colvin VL, Yu WW, Riviere JE. Biodistribution of quantum dot nanoparticles in perfused skin: evidence of coating dependency and periodicity in arterial extraction. Nano Lett 2007;7:2865–70.

[35] Zhu MT, Feng WY, Wang Y, Wang B, Wang M, Ouyang H, et al. Particokinetics and extrapulmonary translocation of intratracheally instilled ferric oxide nanoparticles in rats and the potential health risk assessment. Toxicol Sci 2009;107:342–51.